ELSEVIER

Physica D 85 (1995) 405–424

PHYSICA D

Statistics of temperature increments in fully developed turbulence
Part II. Experiments

M. Ould-Rouis[a], F. Anselmet[a], P. Le Gal[a], S. Vaienti[b,c]

[a]*Institut de Mécanique Statistique de la Turbulence, Unité Mixte Université d'Aix-Marseille II/CNRS N° 380033, 12, Avenue du Général Leclerc, 13003 Marseille, France*

[b]*PHYMAT, Département de Mathématiques, Université de Toulon et du Var, 83957 La Garde Cedex, France*

[c]*Centre de Physique Théorique, Luminy Case 907, 13288 Marseille Cedex 09, France*

Received 7 October 1994; revised 23 December 1994; accepted 13 February 1995
Communicated by U. Frisch

Abstract

A partial differential equation for the probability density function (pdf) of temperature increments in fully developed turbulence has been derived in a previous theoretical analysis [S. Vaienti, M. Ould-Rouis, F. Auselmet and P. Le Gal, Physica D 73 (1994) 99]. This equation is a function of two conditional expectations q_1 and q_2 of respectively the increment of velocity and the temperature dissipation. It was shown that these two quantities are the only parameters that govern the evolution of the pdfs for the temperature increments. With the help of closure hypotheses on q_1 and q_2, the calculation of the asymptotic forms of this pdf is then tractable and displays a notable deviation from the Gaussian behavior for large temperature increment fluctuations when the spatial separation r lies within the inertial and dissipative ranges. The objective of the present paper is to complete our theoretical approach and to investigate experimentally, from simultaneous measurements of velocity and temperature fluctuations obtained in a laboratory wind tunnel, the evolution of the marginal and joint pdfs of the velocity and temperature increments. Attention is particularly paid to the conditional expectations q_1 and q_2.

Dedicated to Valentina

1. Introduction

To interpret the turbulent energy transfer from the large scales to the dissipative ones, Richardson has introduced the fundamental concept of an energy cascade on which is based Kolmogorov's original theory [2]. In fact, experimental observations have pointed out that refined analyses are required to take into account the intermittent nature of the energy transfer towards the small scales, resulting in new models based on various schemes of eddy breakdown [3]. From an experimental point of view, the investigation of the scaling law characteristics through the computation of the high order moments of velocity and temperature increments has shown the complexity of the mechanisms involved in the cascade [4,5]. Therefore, investigations more closely based on the fluid dynamics and its conservation equations are

SSDI 0167-2789(95)00063-1

still needed to improve our understanding of turbulence. Even though this problem has so far received quite little attention, considering a passive scalar advected by the turbulent field is quite attractive since techniques allowing the detailed study of its statistics have been shown to be tractable [6]. An extension of this approach to the prediction of the behavior of temperature increments, or temperature differences $X = \Delta\theta(r) = \theta(x+r) - \theta(x)$ between two points separated by a distance r, has been recently worked out [1]. A similar study has also been recently published [7]. As usual, in the inertial range, the separation distance r is much larger than the Kolmogorov scale η and much smaller than the injection scales – in the dissipative range, r is of order of η. The main theoretical result that we obtained is the explicit partial differential equation of the evolution of the pdf $P(r, \Delta\theta)$ (k_0 is the molecular heat diffusivity):

$$\left(\frac{2}{r} + \frac{\partial}{\partial r}\right)[q_1(r, X)\, P(r, X)] + 2\bar{N}\frac{\partial^2}{\partial X^2}[q_2(r, X)\, P(r, X)] - 2k_0\left(\frac{2}{r} + \frac{\partial}{\partial r}\right)\frac{\partial}{\partial r} P(r, X) = 0\,, \tag{1.1}$$

where $q_1(r, X)$ is the expectation of the increment of velocity $\Delta U(r)$ conditioned by X and $q_2(r, X)$ is the expectation of the dissipation of temperature $k_0 \nabla\theta^2$ conditioned by X. $\bar{N}(=k_0 \overline{\nabla\theta^2})$ is the mean dissipation rate of temperature. Closure hypotheses of the asymptotic behaviors of $q_1(r, X)$ and $q_2(r, X)$ were then made to predict the asymptotic shapes of the pdf $P(r, X)$. The present experimental study is motivated by the determination of the various functions $q_1(r, X)$, $q_2(r, X)$ and $P(r, X)$. Hot wire measurements are conducted in a turbulent boundary layer over a slightly heated wall and Section 2 describes this experimental arrangement. A brief review of the theoretical approach is presented in Section 3 and results are discussed in Section 4. It will be shown that q_1 and q_2 actually quantify very precisely the physical phenomena which are embedded in turbulence and which govern the pdf evolution. Finally, in Section 5, a few additional arguments are given about the universality of the trends we are reporting and about their implications with respect to isotropy.

2. Experimental conditions

2.1. Experimental setup

The study is performed in the turbulent boundary layer developed on the working section floor of a low-speed wind tunnel with a cross section: 0.56×0.56 m^2. This experimental facility has already been investigated quite extensively [8], so that only the flow main characteristics are reported here. The wall is heated from the beginning of the layer to a constant temperature such that the difference with respect to the ambient temperature is 10 K so that temperature is acting as a passive scalar. At the measuring station ($x = 3{,}7$ m), the free stream velocity is $U_e = 12$ m/s, the boundary layer thickness $\delta = 62$ mm and the momentum thickness Reynolds number 4900. The friction velocity is $u^* = 0.46$ m/s. Measurements and exhaustive analyses reported herein are obtained at the non-dimensional distance to the wall $y^+ = 310$ with $y^+ = yu^*/\nu$, ν being the kinematic viscosity of air. At this position, the Reynolds number associated with the Taylor micro-scale is about 180 and the Kolmogorov length-scale is $\eta = 0.13$ mm. In addition, the robustness of our results is demonstrated by complementary studies performed at different points in the same flow, namely, $y^+ = 120$ and $y^+ = 750$, which approximately correspond to the lower and upper limits of the inner region of the boundary layer respectively. Over this range of distances, the flow can be approximately considered as fully turbulent with no direct influence from the limit boundary conditions on the individual statistics of U and θ. When no explicit comment is given, the analysis will be related to the $y^+ = 310$ measurements.

Simultaneous longitudinal velocity u and tem-

perature θ measurements are performed with a pair of parallel wires located at the same distance from the wall. Both wires are etched from wollaston. The upstream cold wire has an active length l of 1 mm and a diameter d of 0.6 μm. The downstream hot wire has an active length of 0.8 mm and a diameter of 5 μm. The streamwise separation between these two wires is about 630 times the cold wire diameter. The hot wire is operated with a constant-temperature circuit at an overheat ratio of 1.6, whereas the cold wire is operated with in-house constant-current circuits. The heating current is adjusted to 0.2 mA so that the velocity sensitivity of the wire is practically negligible and the signal to noise ratio is large enough to allow a correct estimation of temperature increments for small scales r. More details about this arrangement are given in [8].

Both signals are low-pass filtered at a cutoff frequency of 10 kHz which is about the Kolmogorov frequency at this position, before on-line digitizing at 37.5 kHz per channel. The high resolution (15 bits with sample and hold systems) A/D converter is connected to a micro-computer where data (10^6 points corresponding to an about 14 s duration) are stored and processed.

2.2. Validation of turbulence characteristics

The measurement position $y^+ = 310$ has been determined by the optimization of different characteristics of turbulence versus homogeneity and isotropy of the velocity field. In particular, the third order moment of the longitudinal velocity increment has been studied as a function of the scale r. Fig. 1 presents the behavior of this moment and the corresponding mixed moment for temperature, normalized by Kolmogorov velocity and temperature scales and divided by r/η. The velocity curve shows a plateau at the $-4/5$ classical value extending over almost one decade around $r = 80\eta$. This is in accordance with predictions deduced from homogeneity and local isotropy, where the second term in the left hand side is negligible in the inertial range, with

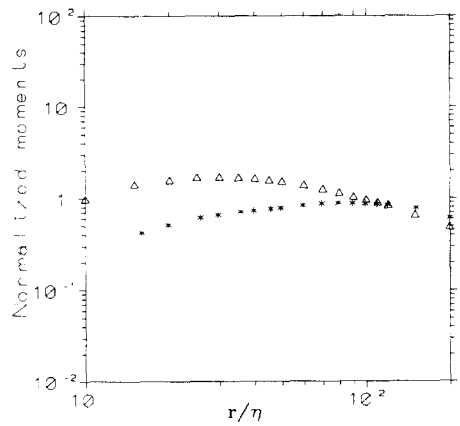

Fig. 1. Variation with the separation r of normalized third order moments, $|\langle(\Delta U)^3\rangle|$ (asterisks) and $|\langle \Delta U(\Delta\theta)^2\rangle|$ (triangles) divided by r/η.

$\bar{\varepsilon}$ the constant mean rate of transfer of kinetic energy:

$$\langle \Delta U^3 \rangle - 2\nu \frac{\mathrm{d}}{\mathrm{d}r} \langle \Delta U^2 \rangle = -\frac{4}{5} \bar{\varepsilon} r \,, \tag{2.1}$$

with $\langle\ \rangle$ denoting an ensemble average. For temperature increments, there is also a plateau region associated with the behavior predicted by the Yaglom formula for the inertial range [9]:

$$\langle \Delta\theta^2 \Delta U \rangle - 2k_0 \frac{\mathrm{d}}{\mathrm{d}r} \langle \Delta\theta^2 \rangle = -\frac{4}{3} \bar{N} r \,. \tag{2.2}$$

However, Fig. 1 shows that the range of the linear scaling law ($10\eta < r < 90\eta$) is slightly shifted towards smaller scales with respect to that obtained for velocity ($30\eta < r < 120\eta$). The position $y^+ = 310$ was selected because it was providing the greatest extent for these plateau regions. In addition, the temperature skewness factor is virtually zero (0.05) and the flatness factor is about 2.8 at this position, corresponding to almost Gaussian conditions. It was also checked that the spectral distributions for the longitudinal velocity U and for the normal to the wall velocity V were in reasonable agreement with the relation resulting from the assumption of local isotropy. Quite similar results were obtained at the two other positions, but the extent of the plateaus was slightly smaller as the

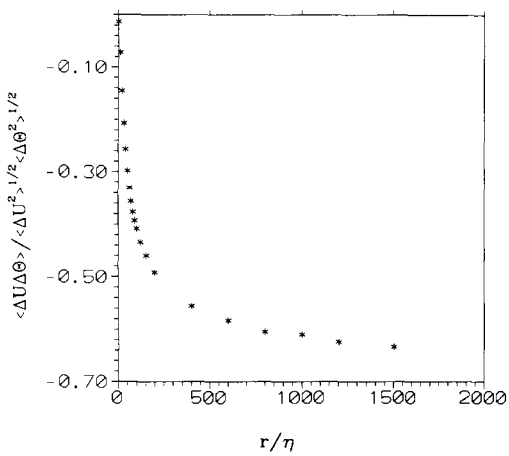

Fig. 2. Evolution with the separation r of the correlation coefficient between ΔU and $\Delta\theta$.

largest Reynolds number R_λ is for $y^+ = 310$. The temperature flatness factor is the same for the three positions, whereas the skewness is also virtually zero (-0.03) at $y^+ = 120$ and positive (about 0.3) at $y^+ = 750$.

We will also finally mention that the wire length influence on the results reported hereafter was carefully checked. Experiments with shorter wires ($l/\eta = 4$) were performed, and the correlation coefficients between ΔU and $\Delta\theta$ were virtually unchanged. However, since short wires ($l/d < 1000$) result in a significant attenuation of the measured temperature variance, it was preferred to use longer wires because our interest mainly lies in the inertial range of scales. Thus, considering also the separation (about 4η) between the cold and hot wires, our results for r/η smaller than about 8 might be approximate though the obtained trends are in complete accordance with conditions imposed by local isotropy, such as the correlation coefficient between ΔU and $\Delta\theta$ going to zero for r/η going to zero (see Fig. 2).

3. Recall of the theoretical analysis

In this section, we briefly recall the main features of our analytical study [1] leading to the evolution equation for the pdf $P(\Delta\theta(r))$ and we also present some extensions very helpful to enlighten our experimental results.

Starting from the diffusion equation for temperature:

$$\frac{\partial\theta(\boldsymbol{x},t)}{\partial t} + \boldsymbol{U}(\boldsymbol{x},t)\cdot\nabla\theta(\boldsymbol{x},t) = k_0\,\nabla^2\theta(\boldsymbol{x},t)\,, \tag{3.1}$$

we have shown in [1] that

$$\left\langle \frac{\partial}{\partial t}\Delta\theta(\boldsymbol{x},t)^n \right\rangle = 0\,, \tag{3.2}$$

where the symbol $\langle\ \rangle$ was used to denote a spatial average over $\boldsymbol{x}\in\mathbb{R}^3$ in analogy with the papers of Yakhot and Sinai [6]. Such a volume measure was implicitly normalized over a large scale L and also assumed was the vanishing of the fields and their derivatives for large values of $\boldsymbol{x}$, say $|\boldsymbol{x}| \sim L$. Finally, the hypothesis of stationarity was also invoked to suppress time derivatives. This and the hypotheses of homogeneity and local isotropy imply that Eq. (3.2) can be transformed as (see [1])

$$\begin{aligned}\frac{1}{\bar{N}\cdot 2n(2n-1)}\left(\frac{2}{r}+\frac{\partial}{\partial r}\right)\langle\Delta\theta^{2n}(\boldsymbol{r},\boldsymbol{x})\,\Delta U(\boldsymbol{r},\boldsymbol{x})\rangle \\ = -2\langle\Delta\theta^{2n-2}(\boldsymbol{r},\boldsymbol{x})\,[\nabla\theta(\boldsymbol{x})]^2\rangle \\ + \frac{k_0}{\bar{N}n(n-1)}\left(\frac{2}{r}+\frac{\partial}{\partial r}\right)\frac{\partial}{\partial r}\langle\Delta\theta^{2n}(\boldsymbol{r},\boldsymbol{x})\rangle\,,\end{aligned} \tag{3.3}$$

where we have rescaled the temperature gradient according to $[\nabla\theta(\boldsymbol{x})]^2 \to [\nabla\theta(\boldsymbol{x})]^2/\langle[\nabla\theta(\boldsymbol{x})]^2\rangle$. $\Delta U(\boldsymbol{r},\boldsymbol{x})$ is the projection of $\Delta\boldsymbol{U}(\boldsymbol{r},\boldsymbol{x})$ along the direction of $\boldsymbol{r}$ and we also set $r = |\boldsymbol{r}|$. In the case $n = 1$, eq. (3.3) reduces to the well-known Yaglom formula (2.2).

We now introduce, following Yakhot and Sinai [6], the stochastic variables on the space $\mathbb{R}^3$ equipped with the volume measure: $X = \Delta\theta(\boldsymbol{r},\boldsymbol{x})$, $Y = \Delta U(\boldsymbol{r},\boldsymbol{x})$ and $Z = [\nabla\theta(\boldsymbol{x})]^2$. Writing the joint pdf $P(r,X,Y,Z)$ as $P(r,X)\ Q(r,Y,Z/X)$, and substituting into (3.3), we get, after having replaced the mean with the distribution

Table 1
Closure expressions for q_1

Zone	$\|X\|$ small	$\|X\|$ large
inertial	$dr^{-\nu}$	$dr^{-\nu}+\gamma_1^+ r^\varepsilon \|X\|^\xi$; $\xi=1,2$
dissipative	dr^χ	$dr^\chi+\gamma_1^+ r^\varepsilon \|X\|$

averaging and by the vanishing of the even moments (see [1] for more detail),

$$\left(\frac{2}{r}+\frac{\partial}{\partial r}\right)[q_1(r,X)P(r,X)] +2\bar{N}\frac{\partial^2}{\partial X^2}[q_2(r,X)P(r,X)] =2k_0\left(\frac{2}{r}+\frac{\partial}{\partial r}\right)\frac{\partial}{\partial r}P(r,X)\,, \tag{3.4}$$

where the conditional expectations $q_1(r,X)$ and $q_2(r,X)$ are defined by

$$q_1(r,X)=\int YQ(r,Y/X)\,\mathrm{d}Y\,,$$

$$q_2(r,X)=\int ZQ(r,Z/X)\,\mathrm{d}Z\,. \tag{3.5}$$

Notice that the conditional probabilities and expectations depend upon the parameter r and not $\boldsymbol{r}$ by isotropy. The function q_1 quantifies the influence of the turbulent velocity field on the transfer of temperature from the large scales to the small ones, whereas q_2 represents the link between temperature and its dissipation, which is known to play an important role in turbulence modelling [10]. The analytical study of (3.4) reported in [1] showed that it is possible to conjecture the analytical form of the closure functions with physical arguments, but also by requiring a certain regularity of the solution of this equation. These closure expressions for q_1 and q_2 are reported in Tables 1 and 2, with $\xi=1$ or 2, $0\leq\beta\leq1$, $\gamma_1^+<0$, and all other exponents positive numbers.

Table 2
Closure expressions for q_2

Zone	$\|X\|$ small	$\|X\|$ large
inertial	$r^\rho(\gamma_2+\gamma_3X^2)$	$r^{-\sigma}(\gamma_2+\gamma_3\|X\|^\beta)$
dissipative	$r^\rho(\gamma_2+\gamma_3X^2)$	$r^{-\sigma}(\gamma_2+\gamma_3\|X\|^\beta)$

Actually, the form of q_2 proposed in [1] was

$$q_2(r,X)=\gamma_2 r^\rho+\gamma_3\frac{|X|^\beta}{r^\sigma}\,,$$

with $\beta=2$ for $|X|$ small, and $0\leq\beta\leq1$ for $|X|$ large (we will explain in a moment the meaning of such attributes for X).

The upper bound for β could be shifted to 2 whenever $q_1(r,X)$ scales asymptotically as $q_1(r,X)\approx\gamma_1^+ r^\varepsilon X^2$ (cf. the appendix). The slightly different expressions for q_2 given in Table 2 capture the dominant asymptotic behavior in the respective regimes and allow also to separate the variables in the solutions of the differential equations for the pdf. Note finally that, in the dissipative range, we get a pdf diverging at the origin [1, Section 5]. The solutions of Eq. (3.4) were studied in [1] by separating the variables in two regimes called $|X|$ small and $|X|$ large. We will consider that $|X|$ is small when it is much smaller than the standard deviation at the considered scale r and, inversely, that $|X|$ is large when it is much larger than the standard deviation. As the variation with r of this standard deviation can be approximated by power law functions both in the inertial and dissipative ranges, our theory directly compares $|X|$ with these functions of r in the chosen unit of measure.

The solution $P(r,X)$ was then factorized as

$$P(r,X)=\phi_\alpha(X)\,\psi_\alpha(r)\,, \tag{3.6}$$

where the sign of the constant α was chosen according to the following rules:
(i) for $|X|$ large, the spatial factor $\phi_\alpha(X)$ must decay to zero,
(ii) for $|X|$ small, the radial factor $\psi_\alpha(r)$ is a decreasing function of r in the dissipative range,
(iii) for $|X|$ large, the radial factor $\psi_\alpha(r)$ is an increasing function of r for r smaller than $|X|$; on the contrary, $\psi_\alpha(r)$ becomes a decreasing function for r much larger than $|X|$.

As an important observation, we showed in [1] that the exponential stretching exhibited by the spatial factor $\phi_\alpha(X)$ is the steepest one compat-

Table 3
Analytical solutions for the two contributions to the pdf associated with the method of separation of variables

Zone	$\|X\|$ small	$\|X\|$ large
inertial	$\phi_\alpha(X) = c\left[1 - \frac{X^2}{\gamma_2}\left(\gamma_3 - \frac{\alpha}{4}\right)\right]$	$\phi_\alpha(X) = c\left(\frac{2\gamma_3}{\alpha}\right)^{1/4} X^{-3(\beta+1)/4} \exp\left(-\frac{2f(\alpha)}{3-\beta} X^{(3-\beta)/2}\right)$
	$\psi_\alpha(r) = cr^{\nu-2} \exp\left(\frac{-\tilde{N}\alpha r^{\nu+\rho+1}}{d(\nu+\rho+1)}\right)$	where $f(\alpha) = (\alpha/2\gamma_3)^{1/2}$
		$\psi_\alpha(r) = \frac{c}{r^{\varepsilon+2}} \exp\left(\frac{-\tilde{N}\alpha}{\gamma_1^+} \frac{r^{1-\varepsilon-\sigma}}{1-\varepsilon-\sigma}\right)$
dissipative	$\phi_\alpha(X) = c\left[1 - \frac{X^2}{\gamma_2}\left(\gamma_3 - \frac{\alpha}{4}\right)\right]$	$\phi_\alpha(X) = c\left(\frac{2\gamma_3}{\alpha}\right)^{1/4} \|X\|^{-3\beta/4} \exp\left(\frac{-2f(\alpha)}{2-\beta} \|X\|^{(2-\beta)/2}\right)$
	$\psi_\alpha(r) = c\left(r^{-1} + \frac{d}{k_0} \ln r + \mathcal{O}(r \ln r)\right)$	where $f(\alpha) = (\alpha/2\gamma_3)^{1/2}$
		$\psi_\alpha(r) = cr^{(\sqrt{1+2\alpha\tilde{N}}-1)/2}$, $\sigma = 2$

ible with an exponentially decaying solution at fixed r.

This asymptotic behavior will be effectively confirmed by the experimental results quoted in Section 4. Table 3 gives the partial solutions of (3.4), deferring to the appendix several comments and explanations; we also slightly changed two notations of the solutions given in [1]. c denotes a constant.

4. Experimental results

4.1. Probability density functions

Simultaneous measurements of temperature and velocity in the turbulent boundary layer, at the position $y^+ = 310$, are used to calculate the velocity and temperature increments, ΔU and $\Delta\theta$ respectively, for different temporal shifts τ through the use of Taylor's hypothesis: $r = -U\tau$. In this section, we will present some results concerning the pdfs of both ΔU and $\Delta\theta$ for various separations r.

As our theory avoids this adimensionalization, we plot (Fig. 3) in semi-logarithmic scales the pdfs of $\Delta\theta$ with their true dimensions for different values of r. When the scale r is decreased, exponential tails are clearly formed. These tails are typical of the intermittent nature of turbulent energy transfer and dissipation at small scales [5, 11, 12]. In the vicinity of $X = 0$, all curves present a parabolic shape with a more or less pronounced peak whose amplitude diverges at $X = 0$ when r goes to zero. The asymptotic form of the pdf as r goes to zero is a delta function, which is not obvious when it is plotted as usually done in its adimensionalized form. Fig. 4 attests this behavior when three-dimensional plots of $P(r, X)$ are used to exhibit the evolution of the pdf with the scale r. As explained in [1], our theory was developed for non-adimensionalized pdfs in order to avoid any assumption for the evolution of $\langle[\Delta\theta(r)]^2\rangle$. Moreover, these second-

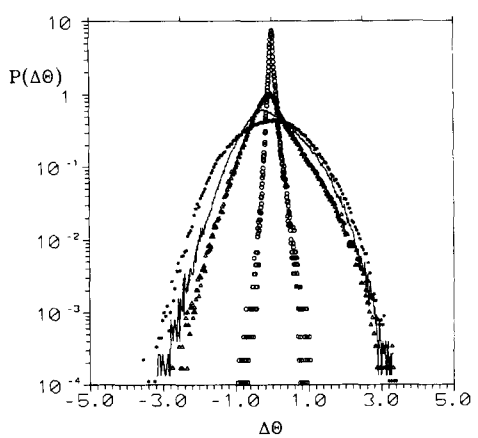

Fig. 3. Pdfs for $\Delta\theta$ in semi-logarithmic scales. Asterisks: $r/\eta = 1000$; full line: $r/\eta = 100$; triangles: $r/\eta = 30$; circles: $r/\eta = 2$.

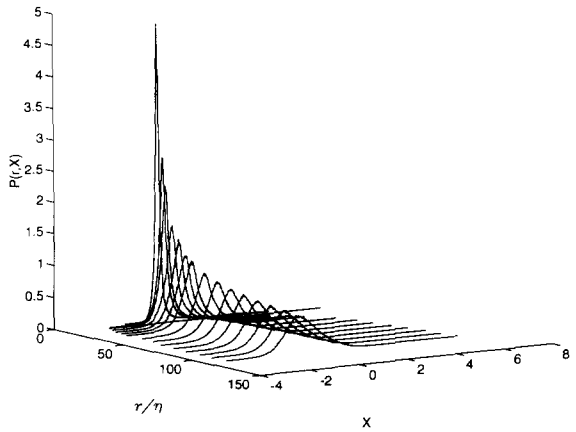

Fig. 4. Three-dimensional representation of the pdfs $P(r, X)$.

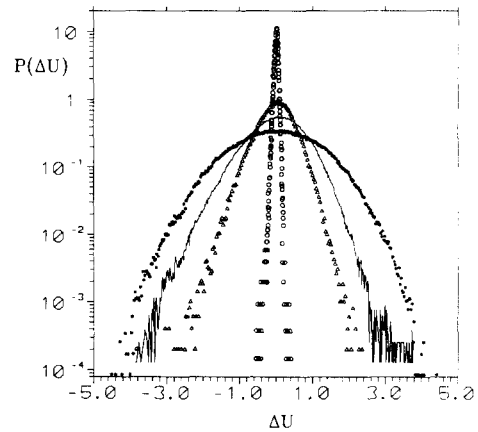

Fig. 5. Pdfs for ΔU in semi-logarithmic scales. Asterisks: $r/\eta = 1000$; full line: $r/\eta = 100$; triangles: $r/\eta = 30$; circles: $r/\eta = 2$.

order moments should be inferred once the pdf equation (3.4) is solved. In the same manner, the conditional averages q_1 and q_2 need to be studied using non-adimensionalized scales in order to examine the predictions given in Tables 1 and 2. In fact, we think that our approach may shed new light on the so far not completely resolved problem associated with the assumption for the variance of the energy transfer rate fluctuations [9, 12]. All of these features will be more quantitatively discussed further along. Let us also note a clear asymmetry in these temperature pdfs which is more pronounced at small r but cannot so far be taken into account by our theory. This behavior seems to result from temperature jumps directly connected to non-zero mean temperature gradients [13].

A similar behavior can be observed for velocity increment pdfs which are presented in Figs. 5 and 6. Although we cannot see the asymmetry as clearly in the velocity pdfs, it also exists. Indeed, Fig. 7 presents – for the three positions $y^+ = 120, 310$ and 750 – the evolution of the absolute value of the skewness factors of the distributions of ΔU and $\Delta\theta$ as a function of r/η in log–log scales. For large separations, both statistics are nearly Gaussian resulting in almost zero skewness factors. As the scale r is decreased, the velocity field evolves towards a non-symmetric distribution in accordance with the local isotropy predictions as described by Eq. (2.1). A plateau is clearly visible over the scales lying within the inertial range. This behavior results directly from the scaling laws of the Kolmogorov theory that gives the theoretical position of this plateau at 0.25, when using the Kolmogorov constant equal to 2.2 [14]. This value is indeed experimentally observed. On the contrary, the small-scale distributions of temperature increments should be symmetric, but as it can be seen, the experimental observations

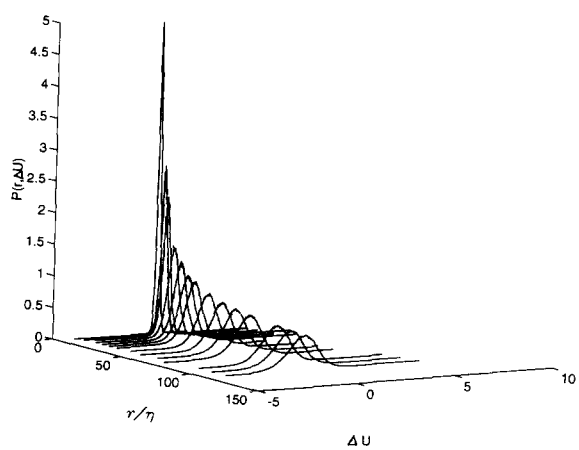

Fig. 6. Three-dimensional representation of the pdfs $P(r, \Delta U)$.

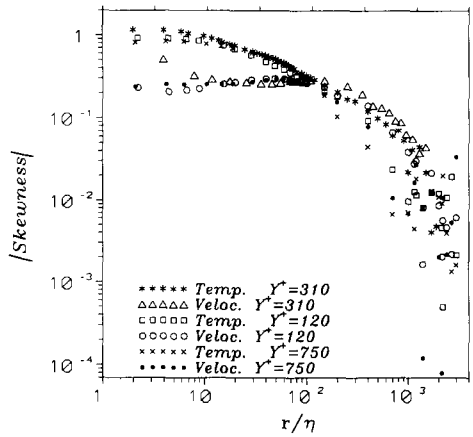

Fig. 7. Variation of the absolute value of the skewness factors of temperature and velocity increments with r.

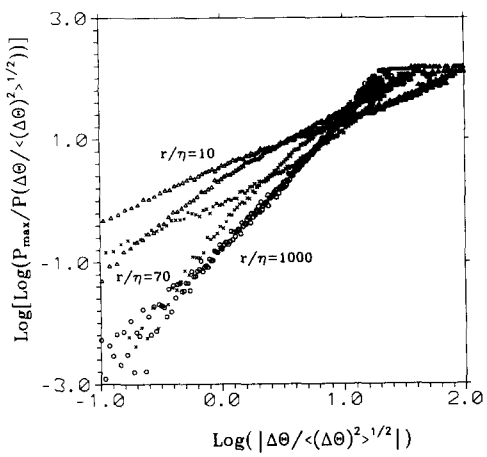

Fig. 8. Stretched exponential forms of the pdfs $P(r, X)$. $r/\eta = 10$; $r/\eta = 70$; $r/\eta = 1000$.

show that the skewness factor strongly departs from zero with an asymptotic value, when r/η tends to 1, of about 1.2, which is in good agreement with that usually obtained for the longitudinal temperature derivative skewness factor (e.g. [15]). The striking observation is the very close correspondence between the statistics of the velocity and temperature fields down to the upper limit of the inertial range where the two skewness factors then separate. Within the inertial range, a scaling law with the exponent $-1/2$ fits quite well the experimental data for the temperature skewness. Using a value of about 2/3 for the power law evolution of $\langle \Delta\theta^2 \rangle$, we thus infer a power law evolution of $\langle \Delta\theta^3 \rangle$ with an exponent close to 1/2. However, isotropy seems to be verified when considering the mixed-moment associated with Eq. (2.2) (see Fig. 1). As a first step, we will not make an attempt at describing precisely this asymmetric feature since our main objective in the present paper is to experimentally validate the theory developed in [1] and the closure assumptions for q_1 and q_2 in order to provide strong guidelines for a numerical study of the pdf evolution equation.

In order to investigate the exact forms of the pdfs' exponential tails, Fig. 8 presents their asymptotic behavior for temperature and different r. Following Ching [11] and our own theoretical analysis (see Table 3), a stretched exponential form, $\exp[-c(r)|X|^{B(r)}]$, can be deduced for any r. To be precise, in our analysis, only two different values of $B(r)$ are allowed, according to whether r belongs to the dissipative or inertial range. As already remarked in [1, Section 5.3], this is a consequence of the fact that we take the exponent β in q_2 independent of r. In order to obtain the function $B(r)$, we compute the quantity $\mathrm{Log}\{\mathrm{Log}[P_{\max}/P(X/\langle \Delta\theta^2 \rangle^{1/2})]\}$ and plot it as a function of $\mathrm{Log}(|X|/\langle \Delta\theta^2 \rangle^{1/2})$ for various separations r. As the pdf is symmetric for large r, both tails collapse on a single line whose slope is slightly larger than 2, in accordance with an almost Gaussian pdf. When r is decreased, the asymmetry of the pdf becomes more and more pronounced. As the tails tend to get separate one from the other, the mean slope is used for $B(r)$. It is obvious from these plots that $B(r)$ increases with r. Indeed, Fig. 9a shows this evolution in more detail. For the injection scales, $B(r)$ is close to 2.5, which is in accordance with the flatness factor F_θ equal to 2.8. Over the scales lying within the inertial zone ($30 < r/\eta < 120$), $B(r)$ is decreased from about 2 to 1. Finally, in the dissipative range, $B(r)$ reaches a value of about 0.75; we note that this exponent is in contradiction with the unicity of the solution

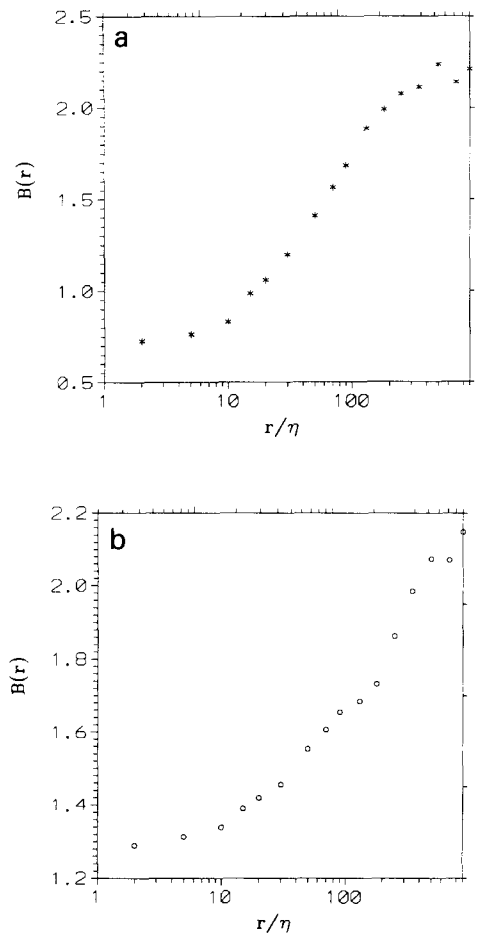

Fig. 9. Exponent $B(r)$ versus r for (a) the temperature and (b) the velocity fields.

of Eq. (1.1). As guessed in [1], we probably have to relax the condition $B > 1$, preventing a subexponential decay of the pdf. Indeed, a different analytic deduction of Eq. (3.4) avoiding the use of moments can relax this constraint [16]. Note that a similar curve is presented in [11] but it is slightly translated downward. In particular, our exponent $B(r)$ is slightly above 0.5, a value previously reported by Gagne [4] and Ching [11]. The resulting evolution of the exponent $B(r)$ versus r, for ΔU, is given in Fig. 9b. This curve presents similar characteristics although the corresponding exponent $B(r)$ undergoes a smaller variation with r: It varies between 1.3 at small scales and 2.2 at large scales. Note finally that, although our theory gives only two values of $B(r)$, in the inertial range it is larger than in the dissipative range, which does not contradict the experimental observations.

4.2. Conditional statistics

In this section, we investigate the evolutions of the conditional expectations $q_1(r, X)$ and $q_2(r, X)$ for different scales r. The corresponding jpdfs are also presented. The coefficients ρ, σ, ν, χ and ε appearing in the analytical forms of q_1 and q_2 are then calculated. Furthermore, we deduce from these results the asymptotic behavior of the pdfs as predicted by our theory, and compare them with experimental fits of the pdfs.

4.2.1. Conditional average $q_1(r, x)$

Fig. 10 presents the jpdfs between ΔU and $\Delta\theta$ plotted on non-dimensional scales for four typical scales r extending from very large ones (injection range, 1000η) to very small ones (dissipative range, 2η). For the largest separation (Fig. 10a), the iso-contour levels of the jpdf are very close to elliptic ones, with their major axes aligned along the second bisectrix: this is characteristic of joint Gaussian pdfs for ΔU and $\Delta\theta$ which are then almost identical to U and θ fluctuations. The corresponding q_1 (see Fig. 11a) is almost perfectly linear, with a slope C equal to the correlation coefficient (-0.6, see [8]) between U and θ; this linear behavior is very close to the expected almost Gaussian property of u and θ but it is in total departure from isotropy. On the other hand, when r is decreased, the shapes of the iso-contours tend to be strongly distorted. This is in good agreement with the general trends on the pdfs reported in Fig. 8. More specifically, the different behaviors previously described are also visible: the temperature field is much more asymmetric than the velocity field, and fluctuations of large magnitudes are more frequent for $\Delta\theta$ than for ΔU, accordingly

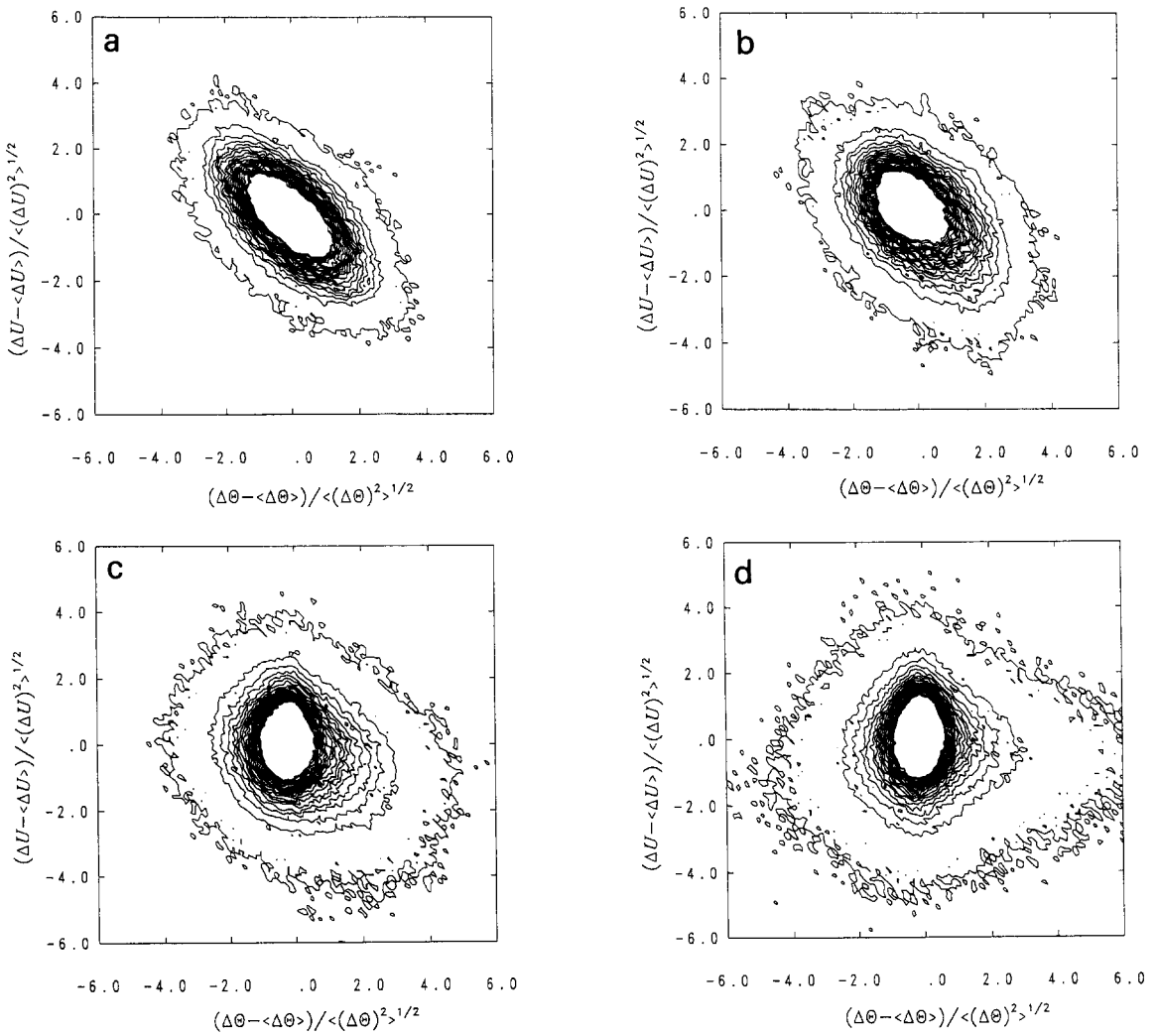

Fig. 10. Normalized joint probability density function between ΔU and $\Delta\theta$. (a) $r/\eta = 1000$; (b) $r/\eta = 100$; (c) $r/\eta = 30$; (d) $r/\eta = 2$. (First contour level: 0.0002; spacing between successive contours: 0.005).

with the smaller exponent $B(r)$ associated with the temperature pdfs' tails (see Fig. 9).

The conditional average q_1 actually provides a quantitative analysis of these evolutions: such results are given in Fig. 11. For large r separations (between 1000η and about 200η), adimensionalized q_1 distributions (Fig. 11a) are almost perfectly linear, with slopes almost constant and very close to C. Then, for smaller separations (roughly those lying within the inertial range), both sides of q_1 have a rather strong evolution, globally corresponding to a strong reduction of the overall slope. However, it is worth noting that the evolution for $X<0$ is much faster in terms of r than that for $X>0$. In particular, for r about 30η, which is the lower limit of the inertial range, the evolution for $X<0$ tends to reverse so that, for scales within the dissipative range, both arms of q_1 are almost completely lying in the $\Delta U<0$ region and the q_1

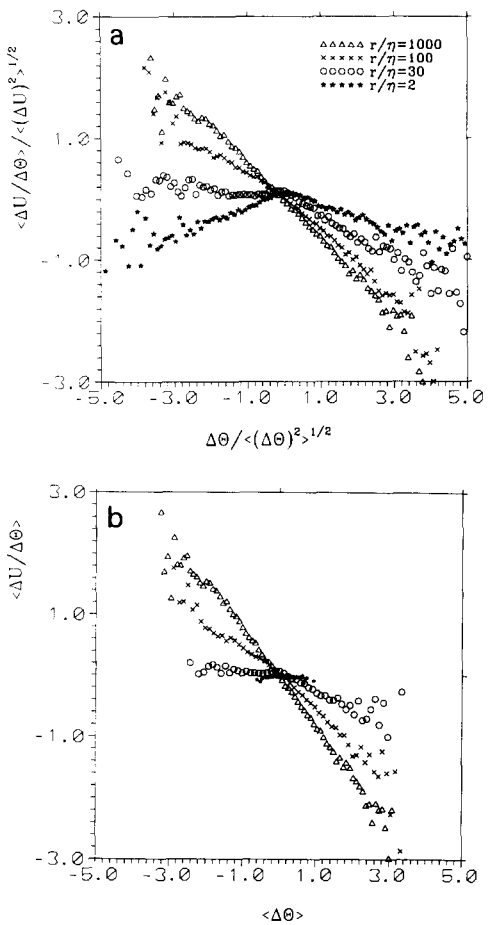

Fig. 11. Evolution of the conditional averages $q_1 = \langle \Delta U / \Delta\theta \rangle$. (a) Normalized q_1; (b) nonnormalized q_1. Triangles: $r/\eta = 1000$; crosses: $r/\eta = 100$; circles: $r/\eta = 30$; stars: $r/\eta = 2$.

distribution has almost an "A" shape, with two arms strongly skewed towards negative ΔU fluctuations. These features are obviously in agreement with the evolution of the correlation coefficient between ΔU and $\Delta\theta$ reported in Fig. 2. They are also in accordance with relation (2.1) as $\langle \Delta U^3 \rangle$ is negative. In order to get analytical expressions for the q_1 behavior to be used for the numerical study of Eq. (3.4), we have searched for asymptotic fits of this quantity that result in the evaluation of coefficients ν and χ for small $|X|$ and ε for large $|X|$. Note that, as explained before, we must also consider all the variables with their true dimensions. Fig. 11b presents the variation of q_1 versus the non-adimensionalized $\Delta\theta$ for various scales r, which naturally displays a much stronger evolution with r than the adimensionalized results of Fig. 11a.

Even though these results concerning joint statistics between the velocity and temperature fields are obtained in a turbulent boundary layer over a heated wall and are obviously strongly influenced by the large-scale boundary conditions, basic considerations on pdfs and moments can be used to demonstrate that the reported final stage for q_1 at small scales is universal. This feature is discussed in more detail in Section 5 where it is shown that q_1 will always possess an "A" shape, regardless of the large-scale conditions which can induce a linear q_1 with either a positive or a negative slope C.

To determine ν and χ, we first set a given value for $X = 0$ and we read $q_1(r, 0)$ as a function of r. The three sets of measurements, corresponding to $y^+ = 120$, 310 and 750, are presented here. As it can be seen, the same behavior is displayed for the three location data. When these results are plotted on log–log scales as a function of r (see Fig. 12a), the dissipative and inertial ranges are clearly characterized by two lines with two different slopes ν and χ, intersecting at $r/\eta = 30$. Regarding exponent ε, we just compute the slopes of $q_1(r, X)$ for large $|X|$ excursions ($X = 2\langle \Delta\theta^2 \rangle^{1/2}$) and for various scales r. Again, the three sets of measurements favorably compare one with the other. We then plot this data (Fig. 12b) which is proportional to $\gamma_1^+ r^\varepsilon$ as a function of r to find the value of the exponent ε. A linear behavior, giving $\varepsilon = 1$, is obtained for the three y^+ positions. Table 4 gathers these results which are those calculated for $y^+ = 310$.

Note that our model, simplified to make the analytical resolution tractable, needs that γ_1^+ changes its sign for $X < 0$ and $r/\eta = 30$. We also note that reported values are in good agreement with the mathematical constraints ($0 \leq \varepsilon \leq 1$ and $\nu \geq 0$ [1]). To investigate the evolution of the

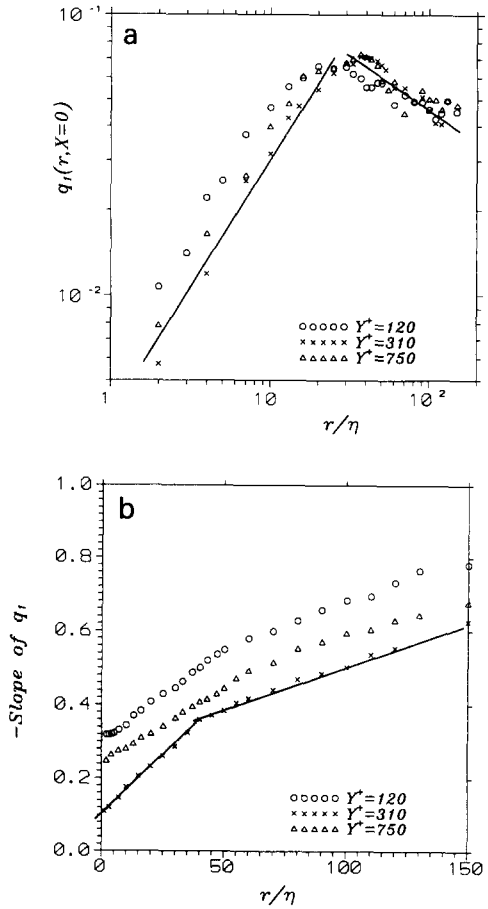

Fig. 12. (a) Evolution of $q_1(r, \Delta\theta = 0)$ with r for the three positions $y^+ = 120$, 310 and 750 (giving exponents $\nu = 0.42$ and $\chi = 0.76$). (b) Evolution of q_1's slope at $|X|$ large (giving exponent $\varepsilon = 1$).

dissipative process governing the pdf evolution, we now need to estimate the coefficients ρ and σ appearing in the analytical expressions of $q_2(r, X)$ as shown by the theoretical approach [1].

Table 4
Experimental estimates of the parameters governing the q_1 evolution

Zone	$\|X\|$ small	$\|X\|$ large
inertial	$\nu = 0.42$	$\varepsilon = 1$
dissipative	$\chi = 0.76$	$\varepsilon = 1$

4.2.2. Conditional average $q_2(r, X)$

Iso-contours for the jpdfs between the temperature increment $\Delta\theta$ and the squared gradient $(\nabla\theta)^2$ show (Fig. 13) that there is also a significant evolution through the scales r of the linkage between these two quantities. For the injection scales, the shape of the jpdf is characteristic of a statistical independence between θ and $(\nabla\theta)^2$ [17]. On the contrary, we recover the parabolic shape corresponding to an exact relation between $\Delta\theta$ and $(\nabla\theta)^2$ when r approaches zero. The resulting conditional average $q_2(r, \Delta\theta) = \langle (\nabla\theta)^2 / \Delta\theta \rangle$ is plotted for various scales r in Fig. 14a. We recall that $(\nabla\theta)^2$ is already normalized by its mean value as we did in the development of the theory. The quantity $q_2(r, X)$ can be approximated by a parabola in the vicinity of $X = 0$, whatever separation r is considered. Indeed, when r goes to zero, an exact parabolic distribution is obtained over the entire X range. But, when r is larger, the extension of the parabolic shape is reduced and it is also reaching smaller values as q_2 only slightly departs from unity. The distribution is flat for the injection scales, resulting from statistical independence between θ and $(\nabla\theta)^2$ [17]. It is interesting to note that our function $q_2(r, X)$ generalizes the conditional expectations q and E defined by Pope and Ching and Valino et al. respectively [18] when studying the relaxation of the pdf of a scalar mixed by a turbulent velocity field. These authors formulate an equation for computing pdfs from these conditional expectations when the transport of the scalar by the velocity field can be neglected. In our case, we explicitly keep this last term – namely, the quantity $(2/r + \partial/\partial r)(q_1 P)$ – since the coupling between the scalar and velocity fields is one of the main ingredients of the mixing process.

In order to investigate the evolutions corresponding to the analytical expressions of $q_2(r, X)$, we must examine q_2 with its true dimension as it is presented in Fig. 14b. We first choose a fixed value of $|X|$ in the vicinity of zero and plot the evolution of $q_2(r, 0)$ for various r

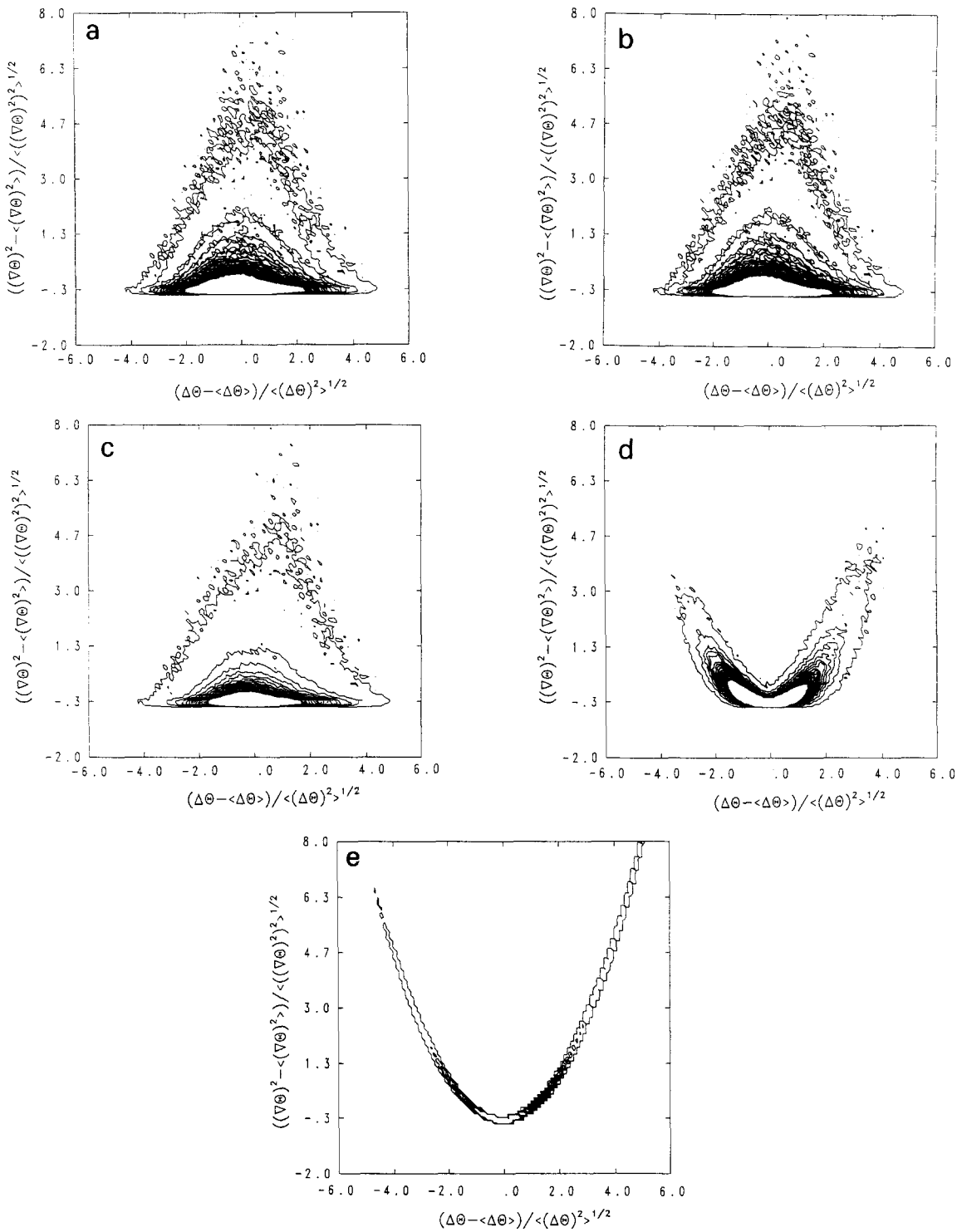

Fig. 13. Normalized joint probability density functions between $(\nabla\theta)^2$ and $\Delta\theta$. (a) $r/\eta = 1000$; (b) $r/\eta = 100$; (c) $r/\eta = 30$; (d) $r/\eta = 3$; (e) $r/\eta = 2$. (First contour level: 0.001; spacing between successive contours: 0.01 for (c), (d) and (e); 0.0002 and 0.005 for (a) and (b)).

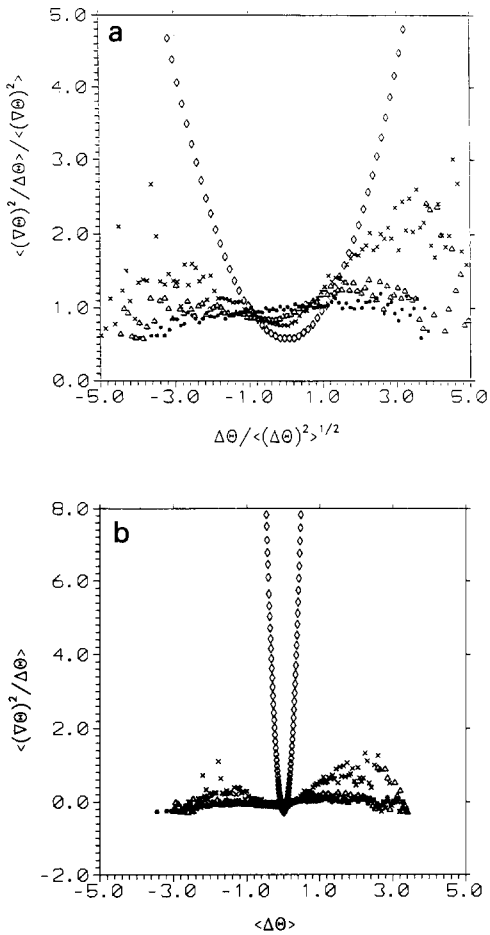

Fig. 14. Evolution of the conditional averages $q_2 = \langle(\nabla\theta)^2/\Delta\theta\rangle$. (a) Normalized q_2; (b) non-normalized q_2. Dots: $r/\eta = 1000$; triangles: $r/\eta = 100$; crosses: $r/\eta = 30$; diamonds: $r/\eta = 2$.

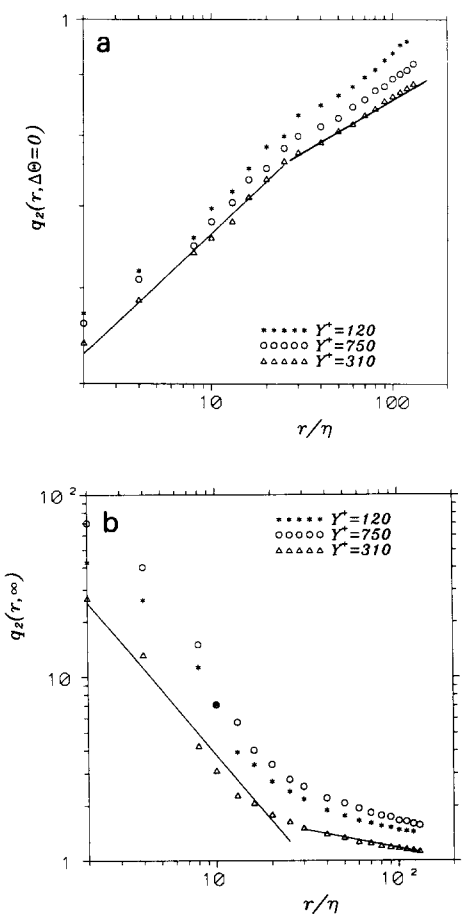

Fig. 15. (a) Evolution of $q_2(r, \Delta\theta = 0)$ with r for the three positions $y^+ = 120$, 310 and 750 (giving exponent $\rho = 0.10$ in the inertial range and $\rho = 0.14$ in the dissipative range). (b) Evolution of $q_2(r, \infty)$ with r for the three positions $y^+ = 120$, 310 and 750 (giving exponent $\sigma = 0.20$ in the inertial range and $\sigma = 1.18$ in the dissipative range).

separations. Here again, results for the three y^+ positions are reported. Fig. 15a shows that a power law evolution is obtained with two distinct lines, intersecting at the separation between inertial and dissipative zones. The slopes of these lines give the researched exponent ρ. In the range of large $|X|$, we also set a prescribed value for X ($X = 1\,K$, which corresponds to several standard deviations for the various separations r), and plotting the corresponding q_2, in log–log coordinates, as a function of r, permits us to determine σ. Fig. 15b presents such results. Indeed, ρ and σ are found to be positive in both ranges of scales. Table 5 presents the experimental coefficients of the analytical expression chosen to model q_2.

Table 5
Experimental estimates of the parameters governing the q_2 evolution

Zone	$\|X\|$ small	$\|X\|$ large
inertial	$\rho = 0.10$	$\sigma = 0.20$
dissipative	$\rho = 0.14$	$\sigma = 1.18$

4.3. Behavior of $P(r, X)$

We will use in this paragraph the values for the various coefficients we have just obtained in order to analyze in a more quantitative way the trends reported in Fig. 3. We will check the validity of our analytical expressions for the pdf $P(r, X)$ – in which coefficients $\varepsilon, \nu, \chi, \rho$ and σ appear – by comparing (Fig. 16) the predicted trends to the experimental results. As the method of separation of variables was the only one to be tractable, we had to write down $P(r, X) = \psi_\alpha(r)\,\phi_\alpha(X)$. We have recalled in Section 3 (see Table 3) the expressions giving $\psi_\alpha(r)$ and $\phi_\alpha(X)$.

In order to consider now the experimental evolutions of the measured pdf, let us first recall the predicted variation with X. When X is small, we naturally recover a quadratic behavior as given in the analytical expression of Table 3. When X is large, the solution $\phi_\alpha(X)$ is characterized by exponential tails, with an exponent B whose study was previously given in Section 4.1. In the inertial range, the experimental value of B varies around 1.5. Let us recall that our sepa-

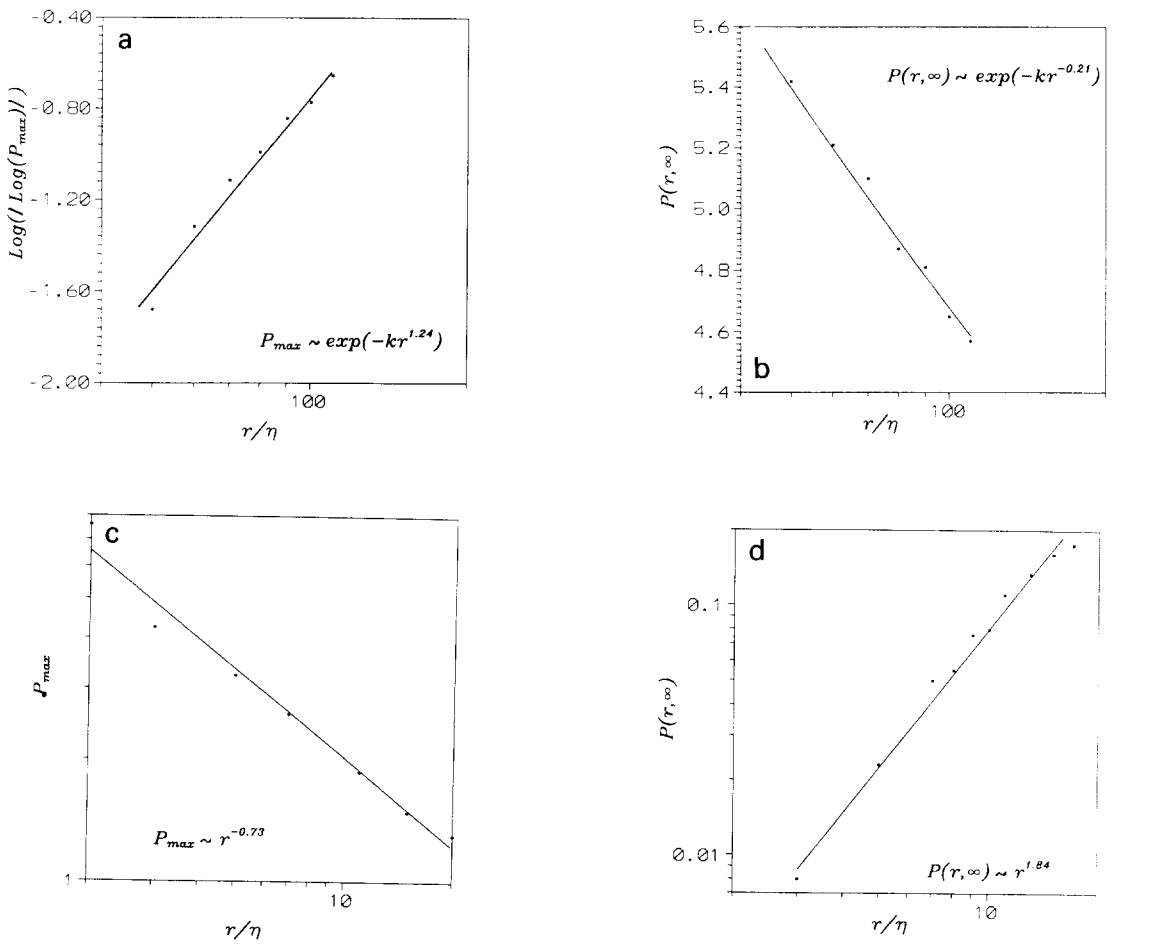

Fig. 16. Fits of the pdf $P(r, X)$ at a fixed X_0. (a) $X_0 \to 0$, inertial zone (giving exponent $1 + \nu + \rho = 1.24$); (b) $X_0 \to \infty$, inertial zone (giving exponent $1 - \varepsilon - \sigma = -0.21$); (c) $X_0 \to 0$, dissipative zone (giving exponent -0.73); (d) $X_0 \to \infty$, dissipative zone (giving exponent 1.84).

ration of variable does not permit in the theory a coefficient β that varies continuously with r. But we find a consistent value of $\beta = 0$ or 1, given by $B = (3-\beta)/2$ or $(4-\beta)/2$ (depending on the expression taken for q_1, see the appendix). In the dissipative range, the experimental value for B is around 0.75, which agrees, according to Table 3, with $\beta = 0.5$. These different values obtained for β are in good agreement with the theoretical requirement that $0 \leqslant \beta \leqslant 1$.

There are 4 cases to be considered to study the evolution of the pdf with r (see Table 3):

(1) In the inertial range and small $|X|$, with the values of the different exponents obtained previously ($\nu = 0.42$, $\rho = 0.10$), $\psi_\alpha(r)$ should behave as $\exp(-Kr^{1.52})$, where K is a positive constant. Fig. 16a shows the variation of $\ln(|\ln(P_{\max})|)$ with $\ln r$, $P_{\max}$ being the maximum value reached by the pdf for the considered scale r. The reported data present, as expected, an almost linear evolution whose slope is the desired exponent. This slope is equal to 1.24 to be compared to the 1.52 prediction.

(2) In the inertial range and for $|X|$ large, again an exponential behavior is predicted. With the values of ε and σ determined before ($\varepsilon = 1$ and $\sigma = 0.20$), the theoretical exponent appearing in the exponential function of r is $1 - \varepsilon - \sigma = -0.20$. Fig. 16b presents, for a fixed value X_0 of X, the variation with r of $\ln\{\ln[P(X_0)]\}$, and shows the expected behavior with an exponent equal to -0.21.

(3) In the dissipative zone for $|X|$ small, the theoretical pdf behavior is given by r^{-1}. A log–log plot of $P_{\max}$ versus r is presented in Fig. 16c, and displays a $r^{-0.73}$ behavior.

(4) In the dissipative zone for $|X|$ large, the prediction is an increasing power law of r. Fig. 16d is in agreement with this theoretical result, giving an exponent equal to 1.84.

To conclude this section, we have shown that the asymptotic behavior of the pdf and of q_1 and q_2 obtained by our analytical study agrees fairly well with the experimental trends.

5. From Gaussianity to isotropy

In order to interpret the behavior of the conditional expectation q_1 and to assess the generality of the previous experimental results, it is worth presenting now some investigations which directly result from mathematical constraints on the pdf $P(r, X)$ and its associated moments. Indeed, homogeneity and local isotropy assumptions induce the following properties on q_1 and q_2. Most of them should be valid for all scales lying within the inertial and dissipative ranges, whereas some of them only hold for the inertial range:

$$\int_{-\infty}^{\infty} q_1 P \, \mathrm{d}X = 0 \quad \text{from } \langle \Delta U \rangle = 0 , \tag{5.1a}$$

$$\int_{-\infty}^{\infty} X q_1 P \, \mathrm{d}X = 0 \quad \text{from } \langle \Delta U \, \Delta\theta \rangle = 0 , \tag{5.1b}$$

$$\int_{-\infty}^{\infty} X^2 q_1 P \, \mathrm{d}X = \langle \Delta U \, (\Delta\theta)^2 \rangle . \tag{5.1c}$$

Associated relations for q_2 inferred from the previous ones using Eq. (3.4) in the inertial range can be obtained.

Eq. (5.1b) is valid because the two fields ΔU and $\Delta\theta$ are uncorrelated at small scales. In fact, in all passive scalar turbulence experiments, these fields are correlated at injection scales, i.e. at large r. Thus, at these scales, local isotropy and homogeneity hypotheses are not verified. If we suppose that the joint statistics between ΔU and $\Delta\theta$ is Gaussian with a correlation coefficient C very close to the correlation between the fluctuations U and θ:

$$q_1 = CX , \tag{5.2}$$

then the right hand side of (5.1b) differs from zero and is equal to C. There is no available prediction for the behavior of this mixed moment, but this quantity is a decreasing function of r. In fact, the forthcoming development will show that ratios of $\langle \Delta U (\Delta\theta)^2 \rangle$ and $\langle \Delta\theta^2 \rangle$ are

involved so that we will not attempt to obtain a precise expression for the evolution of the mixed moment.

As already mentioned in [1], relation (5.2) is in complete violation of local isotropy and homogeneity. The shape of q_1 at scales slightly smaller than the injection scales is then controlled by a process that tends to match together the two statistics: Gaussian at large r, and the statistics of isotropic and homogeneous turbulence at small r. In order to get the very first features of this evolution, we will rewrite (5.2) introducing the small deviation $\Pi(r, X)$ from the Gaussian linear behavior:

$$q_1 = CX + \Pi(r, X) . \tag{5.3}$$

Let us write down a Taylor series expansion of q_1:

$$q_1(X, r) = q_1(0, r) + X\left(\frac{\partial q_1(r, X)}{\partial X}\right)_{X=0} + \frac{1}{2} X^2\left(\frac{\partial^2 q_1(r, X)}{\partial X^2}\right)_{X=0} + \mathcal{O}(|X|^3) . \tag{5.4}$$

We now substitute this expression in Eqs. (5.1), with the integral of (5.1b) being equal to $C\langle X^2\rangle + \langle \Pi(r, X)X\rangle$:

$$q_1(0, r) + \langle X\rangle\left(\frac{\partial q_1}{\partial X}\right)_{X=0} + \frac{1}{2}\langle X^2\rangle\left(\frac{\partial^2 q_1}{\partial X^2}\right)_{X=0} + \cdots = 0 , \tag{5.5a}$$

$$\langle X\rangle q_1(0, r) + \langle X^2\rangle\left(\frac{\partial q_1}{\partial X}\right)_{X=0} + \frac{1}{2}\langle X^3\rangle\left(\frac{\partial^2 q_1}{\partial X^2}\right)_{X=0} + \cdots = C\langle X^2\rangle + \langle \Pi(X)\, X\rangle , \tag{5.5b}$$

$$\langle X^2\rangle q_1(0, r) + \langle X^3\rangle\left(\frac{\partial q_1}{\partial X}\right)_{X=0} + \frac{1}{2}\langle X^4\rangle\left(\frac{\partial^2 q_1}{\partial X^2}\right)_{X=0} + \cdots = \langle \Delta U\, \Delta\theta^2\rangle . \tag{5.5c}$$

Furthermore, as $q_1(X)$ is linear for injection scales, we suppose that when r decreases, $q_1(X)$ deviates slightly from this linear behavior, and we can neglect the contribution from derivatives of order higher than 2. Let us now note that, as $\langle X\rangle = 0$, all first order terms disappear. Plugging expression (5.3) into the truncated equations, we can deduce, at $X = 0$, omitting for simplicity to write explicitly the variation with r, that

$$\Pi(0) + \frac{\langle X^2\rangle}{2}\left(\frac{\partial^2 \Pi(X)}{\partial X^2}\right)_{X=0} = 0 , \tag{5.6a}$$

$$\langle X^2\rangle\left[C + \left(\frac{\partial \Pi(X)}{\partial X}\right)_{X=0}\right] + \frac{\langle X^3\rangle}{2}\left(\frac{\partial^2 \Pi(X)}{\partial X^2}\right)_{X=0} = C\langle X^2\rangle + \langle \Pi(X)\, X\rangle , \tag{5.6b}$$

$$\langle X^2\rangle \Pi(0) + \langle X^3\rangle\left[C + \left(\frac{\partial \Pi(X)}{\partial X}\right)_{X=0}\right] + \frac{\langle X^4\rangle}{2}\left(\frac{\partial^2 \Pi(X)}{\partial X^2}\right)_{X=0} = \langle \Delta U\, \Delta\theta^2\rangle . \tag{5.6c}$$

Combining these three equations, together, we obtain an expression for the second derivative of Π at $X = 0$:

$$\frac{\langle X^2\rangle^2}{2}\left(\frac{\partial^2 \Pi(X)}{\partial^2 X}\right)_{X=0}\left(\frac{\langle X^4\rangle}{\langle X^2\rangle^2} - \frac{\langle X^3\rangle^2}{\langle X^2\rangle^3} - 1\right) = \langle \Delta U\, \Delta\theta^2\rangle - \langle X^3\rangle\left(C + \frac{\langle \Pi(X)\, X\rangle}{\langle X^2\rangle}\right) . \tag{5.7}$$

With the definition of the flatness factor F and the skewness factor S of $\Delta\theta$, Eq. (5.7) then reads

$$\frac{1}{2}(F - S^2 - 1)\left(\frac{\partial^2 \Pi(X)}{\partial^2 X}\right)_{X=0} = \frac{\langle \Delta U\, \Delta\theta^2\rangle}{\langle X^2\rangle^2} - C\frac{\langle X^3\rangle}{\langle X^2\rangle^2} - \langle X^3\rangle\frac{\langle \Pi(X)\, X\rangle}{\langle X^2\rangle^2} . \tag{5.8}$$

In the limit case of nearly Gaussian statistics for the temperature increment field at injection scales, we know the values of its two first moments: $S \sim 0$ and $F \sim 3$. It then follows that

$$\left(\frac{\partial^2 \Pi(X)}{\partial X^2}\right)_{X=0} \approx \frac{\langle \Delta U\, \Delta\theta^2 \rangle}{\langle X^2 \rangle^2}. \tag{5.9}$$

Therefore, whatever the sign of the correlation C, the deviation from linearity of the conditional expectation q_1 is realized with a negative concavity as $\langle \Delta U\, (\Delta\theta)^2 \rangle$ is negative. Consequently, for r very large, the quantity $\langle \Delta U\, \Delta\theta \rangle$ progressively evolves from a linear evolution, with a slope equal to the correlation $C = \langle U\theta \rangle$, towards a curved evolution. Simultaneously, from relation (5.6a), we obtain the evolution of $\Pi(0)$:

$$\Pi(0) \approx -\frac{2\langle \Delta U\, \Delta\theta^2 \rangle}{\langle X^2 \rangle}, \tag{5.10}$$

showing that $q_1(0)$ is getting slightly positive when r is among the injection scales. We predict in this manner that the final shape of q_1, i.e. at sufficiently small scale where turbulence is isotropic and homogeneous, is a chevron with both arms directed downwards as obtained in the previous section. This is true whatever type of turbulence is considered and, in particular, this is independent from the flow boundary conditions which are known to govern the sign of C and, consequently, that of $\langle \Delta\theta^3 \rangle$, for r lying within the inertial range. Thus, we do believe that results previously presented display the universal evolution of q_1.

6. Conclusion

Simultaneous measurements of temperature and velocity have been performed with a two-wire probe in the turbulent boundary layer developing along a heated wall. This data was used to study the statistical distributions of the temperature and velocity increments. Particular attention was devoted to the conditional expectations q_1 and q_2 which govern the evolution of the pdfs for temperature increments. These quantities, together with the pdfs, were calculated for various scales r from the injection range ($r/\eta = 1000$) to the dissipative one ($r/\eta = 2$). These results were more specifically compared with the analytical asymptotic predictions for the pdf $P(r, X)$ of the temperature increment $X = \Delta\theta$ obtained in our previous theoretical study. The robustness of these results was checked by considering three measurement positions within the inner region of the boundary layer where a sufficiently large inertial range exists.

Theoretical assumptions for the scaling laws of q_1 and q_2 are particularly well verified. The asymptotic features display a clear separation between inertial and dissipative ranges occuring at $r/\eta = 30$. Considering the rather low Reynolds number of the experiments, this suggests that our theory enlights the main phenomena governing the mixing action of turbulence. We also proved that, starting from Gaussian statistics at injection scales, the final evolution of q_1 is an "A" shape chevron. We think that this prediction deals with a universal process, that permits the statistics to evolve from "initial" statistics (controlled by the injection scales) to homogeneous and isotropic turbulence statistics. In the same way, the shape of q_2 which controls the dissipation process evolves from a constant horizontal line at injection scales to a parabola at very small scales. These transients through the scales govern the mixing of the temperature field by the turbulent velocity field, and also its dissipation. The shapes of the pdfs are therefore given at various scales r by a search of equilibrium between these two processes.

Our theoretical approach has synthesized the pdf evolution through a partial differential equation (namely Eq. (3.4)). Asymptotic features of the pdf can be obtained by a separation of variables technique, and in particular stretched exponential tails can be detected, in accordance with the experiments. However, it seems that the experimental skewness factor for the distribution of $\Delta\theta$ grows when r is decreased, in total contradiction with the local isotropy assumption which stipulates that it should be zero. This means that, while the velocity field evolves

towards isotropy as $r \to 0$, the scalar field does not obey this trend although the correlation between the velocity and temperature fields actually vanishes when $r \to 0$. This behavior reflects the asymmetry of the pdfs which is very pronounced for temperature increments, and which is so far not taken into account in our model.

Acknowledgements

We are grateful to J. Dusek for fruitful discussions.

Appendix

In this appendix, we comment on Table 3. We first need two remarks. The first one concerns the radial factor $\psi_\alpha(r)$ for large $|X|$ in the dissipative range. In [1] we kept the solution growing as $1/r$, which does not agree with the assumption (ii) in Section 3. To supply for, we observe that $\psi_\alpha(r)$ satisfies the equation (with $\sigma = 1$: we chose $\sigma = 1$ to simplify the computations)

$$\frac{d^2\psi_\alpha(r)}{dr^2} + \frac{2}{r}\frac{d\psi_\alpha(r)}{dr} - \frac{\alpha\bar{N}}{2rk_0}\psi_\alpha(r) = 0\,, \qquad \text{(A.1)}$$

which admits a general solution of the type, in the neighborhood of $r = 0$,

$$\psi_\alpha(r) = A\left(\frac{1}{r} + \frac{\alpha\bar{N}}{2k_0}\ln r + \mathcal{O}(r\ln r)\right) + B\left(1 + \frac{\alpha\bar{N}}{2k_0}\frac{r}{2} + \mathcal{O}(r^2)\right), \qquad \text{(A.2)}$$

with A and B arbitrary constants. By taking $A = 0$, we select a solution bounded in r for small r. To get a solution that effectively goes to zero for $r \to 0^+$, and not to a constant as in (A.2), it will be enough to take $\sigma > 1$ (and not $\sigma = 1$ as in (A.1)). For example, with $\sigma = 2$, the analogue of (A.1) becomes an Euler equation, whose decaying solution is easily found to be

$$\psi_\alpha(r) = \text{const.} \times r^{(\sqrt{1+2\alpha\bar{N}/k_0}-1)/2}\,. \qquad \text{(A.3)}$$

It was just this solution that was quoted in Table 3; clearly, one expects a similar behavior for any $\sigma > 1$.

The second remark concerns the solutions for small $|X|$ in both ranges. In [1], we kept the constant α negative. If, instead, we take $\alpha > 0$, we get for $\phi_\alpha(X)$ a second order expression of the type that is quoted in Table 3:

$$\phi_\alpha(X) = \text{const.} \times \left[\frac{1 - X^2}{\gamma_2}\left(\gamma_3 - \frac{\alpha}{4}\right)\right], \qquad \text{(A.4)}$$

which still gives an asymptotic Gaussian behavior provided that $\alpha < 4\gamma_3$. The radial factor $\psi_\alpha(r)$ has the same form as in Eq. (4.7) in [1] with the property that now $\psi_\alpha(r)$ goes to zero even when $r \to \infty$. Also, the radial part in the inertial range for $|X|$ large goes to zero when $r \to \infty$, since $\varepsilon + \sigma > 1$, as again is found experimentally in Section 4. In the deduction of $\psi_\alpha(r)$ in the dissipative zone, we assumed $q_1 \approx d \approx \text{const.}$; this is not a restriction since we showed in [1] that Eq. (3.4) can be studied in the dissipative regime without the first term on the left hand side containing q_1. Finally we recall that the exponent of X in $\varphi_\alpha(X)$ in the inertial range for $|X|$ large becomes $(4-\beta)/2$ if we take $q_1 \sim \gamma_1^+ r^\varepsilon X^2$. The solution quoted in Table 3 was obtained with $q_1 \sim \gamma_1^+ r^\varepsilon |X|$.

References

[1] S. Vaienti, M. Ould-Rouis, F. Anselmet and P. Le Gal, Physica D 73 (1994) 99.

[2] A.N. Kolmogorov, C.R. Acad. Sci. USSR 30 (1941) 301;
see also U. Frisch, in: Turbulent and Stochastic Processes: Kolmogorov's Ideas 50 Years On (Royal Society, London, (1992) p. 89.

[3] U. Frisch, P.L. Sulem and M. Nelkin, J. Fluid Mech. 87 (1978) 719;

G. Parisi and U. Frisch, in: Turbulence and Predictability in Geophysical Fluid Dynamics (North-Holland, Amsterdam, 1985) p. 84;
R. Benzi, G. Paladin, G. Parisi and A. Vulpiani, J. Phys. A 17 (1986) 3521–3531;
D. Schertzer and S. Lovejoy, J. Geophys. Res. 92 (1987) 9693.

[4] F. Anselmet, Y. Gagne, E.J. Hopfinger and R.A. Antonia, J. Fluid Mech. 140 (1984) 63;
Y. Gagne, Thèse de Docteur ès Sciences, I.N.P. Grenoble (1987);
C. Meneveau and K.R. Sreenivasan, J. Fluid Mech. 224 (1991) 429.

[5] R.A. Antonia, E.J. Hopfinger, Y. Gagne and F. Anselmet, Phys. Rev. A 30 (1984).

[6] Y.G. Sinai and V. Yakhot, Phys. Rev. Lett. 63 (1989) 1962;
V. Yakhot, Phys. Rev. Lett. 63 (1989) 1965.

[7] R.H. Kraichnan, Phys. Rev. Lett. 72 (1994) 1016.

[8] F. Anselmet, R.A. Antonia, T. Benabid and L. Fulachier, in: Structure of Turbulence and Drag Reduction (Springer, Berlin, 1990) p. 349, and references herein.

[9] A.S. Monin and A.M. Yaglom, Statistical Fluid Mechanics, Vols. 1 and 2 (MIT Press, Cambridge, MA, 1975).

[10] V. Eswaran and S.B. Pope, Phys. Fluids 31 (1988) 506; H. Chen, S. Chen and R.H. Kraichnan, Phys. Rev. Lett. 62 (1989) 2657.

[11] E.S. Ching, Phys. Rev. A 44, 6 (1991) 3622.

[12] B. Castaing, Y. Gagne and E.J. Hopfinger, Phys. D 46 (1990) 177.

[13] A. Pumir, Phys. Fluids 6 (1994) 2118.

[14] A. Praskovsky and S. Oncley, Phys. Fluids 6 (1994) 2886.

[15] K.R. Sreenivasan, Proc. R. Soc. London A 434 (1991) 165.

[16] J. Dusek, private communication.

[17] F. Anselmet, H. Djeridi and L. Fulachier, J. Fluid Mech. 280 (1994) 173.

[18] S.B. Pope and E.S. Ching, Phys. Fluids 5 (1993) 1529; L. Valino, C. Dopazo and J. Ros, Phys. Rev. Lett. 72 (1994) 3518.